Journal of Medicinal Chemistry

pubs.acs.org/jmc

Article

Characterization of Chlorogenic Acid as a Two-Photon Fluorogenic Probe that Regulates Glycolysis in Tumor Cells under Hypoxia

Qinghua Wang, Qingyang Zhang, Zhihui Zhang, Ming Ji, Tingting Du, Jing Jin, Jian-Dong Jiang, Xiaoguang Chen,* and Hai-Yu Hu*

Cite This: *J. Med. Chem.* 2023, 66, 2498−2505

Read Online

ACCESS | Metrics & More | Article Recommendations | Supporting Information

ABSTRACT: High levels of steady-state mitochondrial reactive oxygen species (ROS) and glycolysis are hallmarks of cancer. An improved understanding of interactions between tumor energetics and mitochondrial ROS modulation is useful for the development of new anticancer strategies. Here, we show that the natural product chlorogenic acid (**CGA**) specifically scavenged abnormally elevated mitochondrial $O_2^{\bullet-}$ and exhibited a two-photon fluorescence turn-on response to tumor cells under hypoxia and tumor tissues *in vivo*. Furthermore, we illustrated that **CGA** treatment reduced $O_2^{\bullet-}$ levels in cells, hampered activation of AMP-activated protein kinase (AMPK), and shifted metabolism from glycolysis to oxidative phosphorylation (OXPHOS), resulting in inhibition of tumor growth under hypoxia. This study demonstrates an efficient two-photon fluorescent tool for real-time assessment of mitochondrial $O_2^{\bullet-}$ and a clear link between reducing intracellular ROS levels by **CGA** treatments and regulating metabolism, as well as undeniably helpful insights for the development of new anticancer strategies.

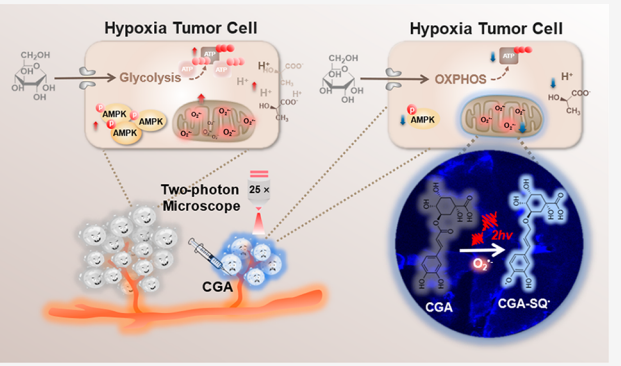

INTRODUCTION

Cancer metabolism is increasingly relevant to cancer research as cancer cells exhibit numerous alterations in aerobic glycolysis, reduced oxidative phosphorylation, and increased production of biosynthetic intermediates that are required for cell growth and proliferation.[1−4] High steady-state reactive oxygen species (ROS) levels influence cancer development and its response to therapies.[5−8] Superoxide anions ($O_2^{\bullet-}$) are a predominant ROS and act as integrators of environmental information as well as downstream effectors of signaling pathways.[9−11] Thus, more insights into interactions between energetics metabolism and ROS in tumorigenesis can contribute to new cancer therapies. However, the interactions between energetics metabolism and ROS homeostasis in cancer cells are difficult to study via analysis of transcript or protein expression levels alone. Moreover, their analysis by traditional biochemical approaches, such as chromatography, mass spectrometry, enzymatic cycling assays, capillary electrophoresis, and isotope-labeling techniques, is *in vitro*, invasive, and not able to capture the transient subcellular ROS changes associated with metabolic activation in cancer cells.[12] Methods employing fluorescent small molecules that rapidly and directly visualize analytes of interest are therefore an alternative *in situ* approach for dissecting ROS−energy metabolism interactions in intact living cells and *in vivo*, which is critical for interrogating cancer cell functions and will provide helpful insights for developing new strategies to prevent or treat cancer.

Fluorescence imaging is a widely used powerful tool to visualize important biological events in living cells *in situ* in a real-time manner, which has extraordinarily high selectivity, sensitivity, and spatial resolution.[13−16] Compared to one-photon fluorescence imaging, two-photon fluorescence imaging has the advantages of outstanding resolution, deep tissue penetration, and minimal photobleaching and photodamage.[17−19] Two-photon fluorescence imaging, based on the turn-on strategy, provides reliable, direct, and noninvasive imaging of various biological applications.[20−22] However, theranostic agents that can both image and regulate the energy metabolic activities of cancer cells are rare.

Numerous plants, including fruits, vegetables, and coffee beans, biosynthesize chlorogenic acid (**CGA**), an ester formed from caffeic acid and L-quinic acid.[23−25] **CGA** is a drug used to treat patients with glioma in phase II clinical trials (NCT03758014, Nov. 2018). However, the molecular mechanisms of its anticancer bioactivity remain unknown.

Received: August 12, 2022
Published: February 6, 2023

https://doi.org/10.1021/acs.jmedchem.2c01317
J. Med. Chem. 2023, 66, 2498−2505

Here, we demonstrate that **CGA** naturally reacted with $O_2^{\bullet-}$ to form **CGA-SQ**$^{\bullet}$. Furthermore, modulating levels of mitochondrial $O_2^{\bullet-}$ reacting with **CGA** regulated glycolytic pathways in tumor cells under hypoxia. The reaction of **CGA** with $O_2^{\bullet-}$ showed a strong two-photon fluorescence emission turn-on response and can hence be an efficient two-photon fluorogenic probe for specific detection of mitochondrial $O_2^{\bullet-}$ activity in both tumor cells and tissues *in vivo* (Scheme 1).

Scheme 1. Luminescence Mechanism of CGA with $O_2^{\bullet-}$

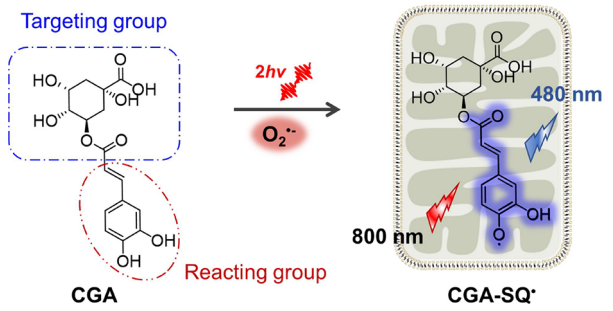

RESULTS AND DISCUSSION

Evaluation of the Photophysical Properties of CGA. The natural product **CGA** is the ester of caffeic acid and quinic acids. Inspired by the antioxidative activity of **CGA** and the fluorescence responses of caffeic acid segments to $O_2^{\bullet-}$,[26] we hypothesized that **CGA** was a caffeic acid-based two-photon fluorescent imaging probe that can specifically capture $O_2^{\bullet-}$ and exhibited a fluorescence turn-on response. To prove our hypothesis, we first investigated the photophysical properties of **CGA** and its fluorescence responses to $O_2^{\bullet-}$ *in vitro*. As shown in Figure 1a, **CGA** exhibited maximal absorption wavelengths at ca. 330 nm, which shifted to 410 nm upon the addition of $O_2^{\bullet-}$. Likewise, the fluorescence intensities of **CGA** at 480 nm were linearly enhanced by the addition of up to 5.0 μM of $O_2^{\bullet-}$ (Figure 1b) and the linear regression equation was F = 10,233 [$O_2^{\bullet-}$] (μM) + 1189.9 with a correlation coefficient of 0.9904. Using the equation LOD = 3σ/K, the detection limit was calculated as 0.54 μM (Figure 1c). This reaction with $O_2^{\bullet-}$ and conversion to **CGA-SQ**$^{\bullet}$ was further identified by ^{1}H NMR spectral analysis, electron spin resonance (ESR) spectroscopy, HPLC−MS analyses, geometry and spin density distribution study, and computer simulations (for details, see Schemes S1 and S2 Figures S1−S6). To verify the specificity of **CGA** to $O_2^{\bullet-}$, we performed its response to other competing ROS, including reactive nitrogen species (RNS) and metal ions. As shown in Figure 1d, the addition of these competitors barely altered the fluorescence intensity of **CGA**, indicating that **CGA** specifically reacts with $O_2^{\bullet-}$. A pH titration experiment showed that **CGA** fluorescence intensity remained unchanged at pH 6.0−8.0 (Figure S7). Taken together, **CGA** is a potential tool for highly sensitive assessments of the concentration of $O_2^{\bullet-}$ under physiological conditions.

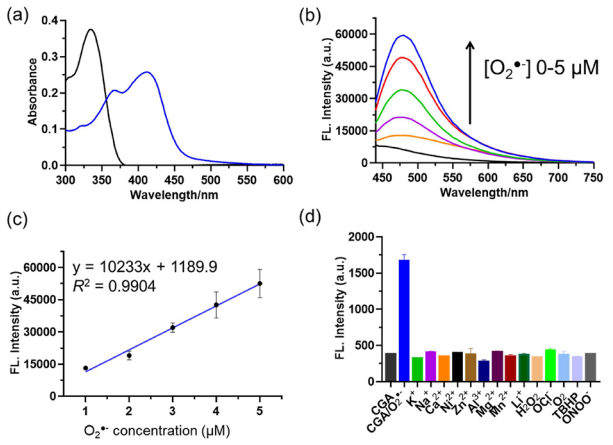

Figure 1. The optical properties and selectivity of **CGA**. (a) Absorption spectra of 20 μM **CGA** (black) and 20 μM **CGA** incubated with $O_2^{\bullet-}$ (blue). (b) Fluorescence spectra of 20 μM **CGA** with different concentrations of $O_2^{\bullet-}$. (c) Calibration curve of fluorescence intensities versus $O_2^{\bullet-}$ concentrations. (d) Fluorescence intensity of 20 μM **CGA** after adding different potential interferences ($O_2^{\bullet-}$ (XO/HPX), 10 mM K^+, 10 mM Na^+, 100 μM Ca^{2+}, 100 μM Ni^{2+}, 100 μM Zn^{2+}, 100 μM Al^{3+}, 100 μM Mg^{2+}, 100 μM Li^+, 10 mM H_2O_2, 100 μM NaClO, 100 μM $^1O_2$, 100 μM TBPH, 1 μM $ONOO^-$). Spectra were acquired at $\lambda_{ex/em}$ = 400/480 nm. Data show the mean ± SD.

Utilization of CGA for Imaging Live Cells. To determine whether **CGA** can effectively function *in vivo*, we first used it to visualize $O_2^{\bullet-}$ in living cancer cells. 2-Methoxyestradiol (2-ME) increases $O_2^{\bullet-}$ concentrations by inhibiting copper-zinc or manganese superoxide dismutase. Ascorbic acid (Vc) and superoxide dismutase (SOD) as an antioxidant suppresses ROS production.[27] Thus, A375 melanoma cells were pre-treated with 2-ME to induce oxidative stress. As illustrated in Figure 2b, remarkable blue fluorescent signal enhancement was obtained in 2-ME-treated melanoma cells compared to the control (Figure 2a), due to the raising of $O_2^{\bullet-}$ concentrations. After the addition of 1.0 mM Vc or 20.0 U/mL SOD to these cells, the fluorescence intensities decreased immediately, which indicates redox reversibility (Figure 2c,d, Figures S8 and S9). Thus, the blue

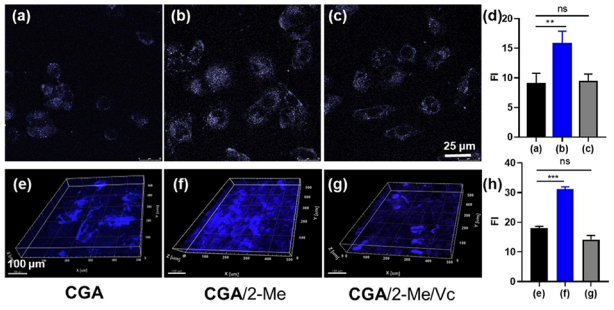

Figure 2. Fluorescence images of $O_2^{\bullet-}$ levels in human cancer cells and mice. (a) A375 cells were incubated with 10 μM **CGA** for 30 min. (b) A375 cells shown in (a) were then treated with 2-ME (1.0 μg/mL). (c) A375 cells shown in (b) were subsequently incubated with 1.0 mM Vc. (d) The average fluorescence intensity histograms from images a−c. (e−h) Two-photon 3D images of $O_2^{\bullet-}$ levels in tumor of mice. (e) A375 tumor in mice. (f) 2-ME-treated A375 tumor in mice and (g) Vc-treated A375 tumor of 2-ME stimulated mice following 10 μM **CGA** injection. (h) The average fluorescence intensity histograms from images e−g. Fluorescence images were captured under excitation with an 800 nm laser light. 3D images (second row) were synthesized by a stack of cross sections (*xy* sections, 500 μm) with an axial (*z*) increment of 60 μm. Fluorescence emission windows (λ_{em} = 420 to 460 nm). Scale bar = 100 μm. The bar graphs show the mean ± SD. *p < 0.05; **p < 0.01; ***p < 0.001.

https://doi.org/10.1021/acs.jmedchem.2c01317
J. Med. Chem. 2023, 66, 2498−2505

fluorescence of **CGA** changed with $O_2^{\bullet-}$ concentrations. Taken together, these results demonstrated **CGA** selectively and reversibly reacts with $O_2^{\bullet-}$ within cells.

Next, we examined the $O_2^{\bullet-}$ levels in tumor tissues in tumor-bearing mice (A375 melanoma, BALB/c-nu) using two-photon fluorescence imaging. As before, we used 2-ME and Vc to alter $O_2^{\bullet-}$ concentrations. Consistent with the observation in cell cultures, stronger fluorescence was detected in tumor tissues treated with 2-ME when compared to the control and the fluorescence intensities significantly decreased with subsequent Vc treatment, indicating a respective increase and decrease in $O_2^{\bullet-}$ concentrations (Figure 2e–h, Figure S10).

Mitochondria Apparatus Localization of CGA. The mitochondrial respiratory chain is a major source of $O_2^{\bullet-}$.[28,29] In the structure of **CGA**, quinic acid is presumed as a mitochondria-targeting group as it activated Ca^{2+}-dependent mitochondrial function.[30] To determine whether **CGA** was specifically activated in the mitochondrial apparatus, an imaging experiment is performed. 2-ME-pre-treated A375 melanoma cells were cultured in media supplemented with **CGA** and commercial organelle dyes (MitoTracker Green and LysoTracker Red). The overlapped fluorescence images in Figure 3a showed that **CGA** fluorescence corresponded with

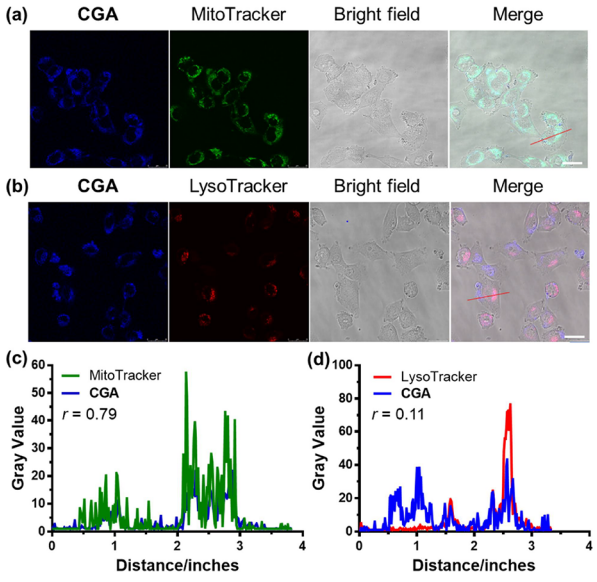

Figure 3. Representative confocal images of intracellular colocalization studies of **CGA** (10 μM) incubated with 2-Me (1.0 μg/mL) pretreated A375 cells co-stained with (a) MitoTracker Green (λ_{ex} = 488 nm, λ_{em} = 530–535 nm) and (b) LysoTracker Red (λ_{ex} = 577 nm, λ_{em} = 580–620 nm). (c, d) Plots depict fluorescence intensity profiles along straight red lines. Pearson's correlation coefficient for **CGA** was calculated at 0.79 for MitoTracker and 0.11 for LysoTracker. Scale bar = 25 μm.

that of MitoTrack Green and Pearson's colocalization coefficient was 0.79 (Figure 3c). However, no fluorescence inside lysosomes was observed under the treatment of **CGA** (Figure 3b,d, colocalization coefficient 0.11). Taken together, these data indicated that **CGA** predominantly accumulates in the mitochondria apparatus and reflects the mitochondria $O_2^{\bullet-}$ level.

CGA Attenuated the Glycolytic Phenotypes under Hypoxia. AMPK, a cellular energy sensor, plays a pivotal role in cancer energy metabolism.[31,32] Targeting ROS by manipulating AMPK activity and reprogramming the glucose metabolic pathway is a recently developed therapeutic strategy.[33] However, therapeutic agents that directly link mitochondrial $O_2^{\bullet-}$ modulation and reprogramming of tumor energetics are rare. Glioma cancer cells treated with **CGA** had not only reduced proliferation rates but also migration/invasion abilities and decreased ATP production in mitochondria.[34] Therefore, we hypothesized that **CGA** is a putative therapeutic and diagnostic agent that mediates ROS–energy metabolism and images and regulates the energy metabolic activities of cancer cells. Solid tumors are characterized by hypoxia, which triggers increased mitochondrial ROS production and leads to AMPK activation.[35–37] Therefore, we investigated the therapeutic effect of **CGA** in cell cultures under hypoxic conditions compared to normoxia. The effects of different **CGA** concentrations (1.25–10 μM **CGA**) on the viability of A375 melanoma cells under normoxic (20% O_2) or hypoxic (1% O_2) conditions were assessed by MTT (3-(4,5-dimethylthiazol-2-yl)-2,5-diphenyltetrazolium bromide) assays and compared to untreated control. As shown in Figure 4a,b, **CGA** treatment was effective under hypoxia whereas its growth inhibitory effect was lost under normoxia, suggesting that **CGA** exhibits hypoxia-dependent anticancer activity. Additionally, colony formation assays verified this hypoxia-

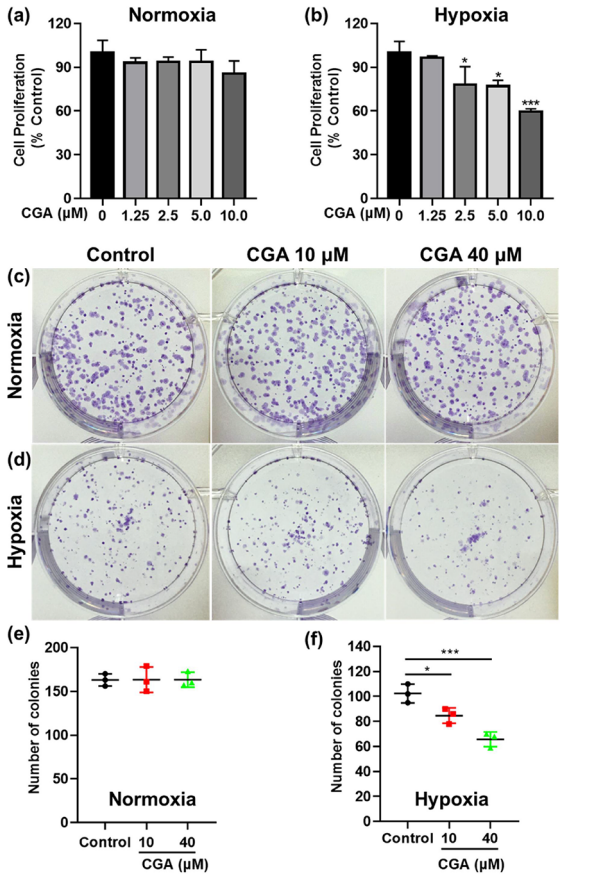

Figure 4. CGA suppressed the proliferative ability of melanoma cancer cells. (a, b) A375 cells were incubated with 0–10 μM **CGA** for 72 h under normoxia and hypoxia. (c–f) Six-well plates were inoculated with A375 cells (300 cells/well) and then treated with 10 and 40 μM **CGA**. Cells were cultured for 10 days under normoxia and hypoxia. Each experiment was reproduced at least thrice. The bar graphs show the mean ± SD. *p < 0.05; **p < 0.01; ***p < 0.001.

https://doi.org/10.1021/acs.jmedchem.2c01317
J. Med. Chem. 2023, 66, 2498–2505

dependent anticancer activity of **CGA**, as indicated by the significantly reduced colony numbers. In contrast, no significant difference was observed between **CGA**-treated and control groups under normoxia (Figure 4c–f).

Furthermore, to evaluate cancer cell susceptibility to **CGA** *in vivo*, we created xenografts from A375 melanoma cells. As shown in Figure 5a–c, **CGA** effectively inhibited tumor growth without any obvious effect on body weight. Tumors from both the 50 mg/kg **CGA**-treated group and control were collected at the end of the efficacy experiment and subjected to Western blot analysis. Figure 5d and Figure S11 demonstrate how **CGA** treatment resulted in a decrease in AMPKα phosphorylation (p-AMPK) at Thr172 in tumor tissues. Taken together, these data illustrated that **CGA** possibly decreases tumorigenicity by regulating energy metabolism under hypoxic conditions.

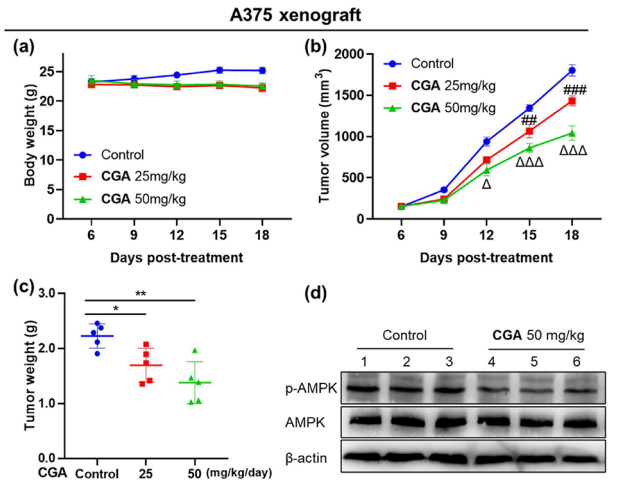

Figure 5. Intraperitoneally administered **CGA** eliminates A375 xenograft. (a) Body weights were determined during treatments. (b) Tumor volumes were determined during treatments. (c) Tumor weights of vehicle control, **CGA** 25 mg/kg, and **CGA** 50 mg/kg were determined. (d) Western blot analysis of phospho-AMPK(Th172) (p-AMPK) and total AMPK expressions from the vehicle control group and **CGA** 50 mg/kg group. The bar graphs show the mean ± S.D. $^{*}p < 0.05$; $^{**}p < 0.01$; $^{\#\#}p < 0.01$, $^{\#\#\#}p < 0.001$ control vs **CGA** 25 mg/kg; $^{\Delta}p < 0.05$, $^{\Delta\Delta\Delta}p < 0.001$ control vs **CGA** 50 mg/kg.

To elucidate the anticancer molecular mechanisms of **CGA**, A375 melanoma cells under hypoxia were treated with **CGA** and levels of $O_2^{\bullet-}$ were quantified by flow cytometry using dihydroethidium (DHE) as a redox-sensitive probe. As illustrated in Figure 6a,b, **CGA** treatment decreased $O_2^{\bullet-}$ activities since the electron-donating catechol of caffeic acid residue in **CGA** was oxidized and formed the semiquinone free radical **CGA-SQ**$^{\bullet}$, resulting in the consumption of $O_2^{\bullet-}$. However, levels of $O_2^{\bullet-}$ have no significant change between the **CGA**-treated and control groups under normoxic conditions (Figure S12). The results of the Western blot showed reduced phosphorylated AMPK expression levels in A375 melanoma cells treated with **CGA** when incubated under hypoxic conditions (Figure 6c, Figure S13). However, under normoxic conditions, AMPK Thr172 phosphorylation in A375 melanoma cells increased after incubation with **CGA** (Figure S14). To determine the influence of **CGA** treatment on energy metabolism in cancer cells under oxidative stress, we tested extracellular acidification rates (ECAR), oxygen consumption rates (OCR), and ATP production in A375 melanoma cells under hypoxia vs normoxia. Compared to the control, ECAR and ATP production dramatically decreased whereas OCR increased in cells under hypoxia that was treated with **CGA** (Figure 6d–f, Figures S15–S18). However, no significant difference was observed between the **CGA**-treated and control groups under normoxic conditions (Figures S19–S23). Taken together, under hypoxic conditions, **CGA** reduced levels of $O_2^{\bullet-}$, hampered the activation of AMPK, shifted metabolism from glycolysis to OXPHOS, and ultimately effectively inhibited the proliferation of cancer cells both *in vitro* and *in vivo*.

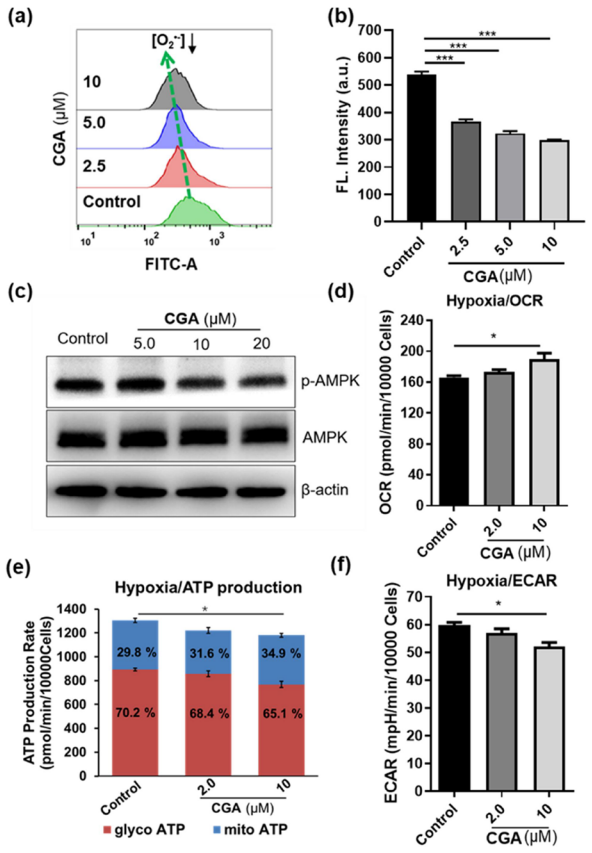

Figure 6. CGA attenuated the glycolytic phenotypes under hypoxia. (a) The levels of extracellular $O_2^{\bullet-}$ under treatment with **CGA** were measured by flow cytometry. (b) Quantification of extracellular $O_2^{\bullet-}$ by FACS analysis. (c) Western blot analysis of proteins associated with phospho-AMPK(Th172) and total AMPK expressions in A375 cells treated with **CGA** (0, 5.0, 10, and 20 μM) for 72 h. The density value of each band was normalized to β-actin level and expressed relative to the control. (d) Extracellular acidification rate of A375 cells after incubating with 0, 2.0, and 10 μM **CGA** concentrations for 6 h. (e) The proportion of ATP generated from mitochondrial oxidative phosphorylation (mito ATP) versus that produced by glycolysis (glyco ATP), both calculated using the real-time ATP rate assay. (f) O_2 consumption rate in A375 cells cultured in 0, 2.0, and 10 μM **CGA** concentrations for 6 h. The results are representative of three independent experiments. The bar graphs show the mean ± SD. $^{*}p < 0.05$; $^{**}p < 0.01$; $^{***}p < 0.001$.

CONCLUSIONS

In summary, we explored a caffeic acid-based natural product (**CGA**) as a two-photon fluorescent probe to image mitochondrial $O_2^{\bullet-}$. This probe facilitates us to image mitochondrial $O_2^{\bullet-}$ in living tumor cells and tissues *in situ* and real time due to its advantages of the instantaneous and highly sensitive response. Furthermore, we showed that **CGA**

https://doi.org/10.1021/acs.jmedchem.2c01317
J. Med. Chem. 2023, 66, 2498−2505

inhibited activation of AMPK, altered cancer metabolic phenotypes, and had *in vitro* and *in vivo* anti-proliferative bioactivity. These findings have increased insights into the role of the mitochondrial $O_2^{\bullet-}$ in cancer energy metabolism. Accurate detection of mitochondrial $O_2^{\bullet-}$ levels changes in cancer cells and will provide a more comprehensive understanding of tumor pathogenesis regarding cancer energy metabolism, which assists with the identification of novel targets in cancer treatment. Further studies will be forced on the fishing and identifications of the direct target of **CGA**.

EXPERIMENTAL SECTION

Materials and Reagents. **CGA** was kindly provided by Jiuzhang Biotechnology Ltd., Inc. (Sichuan, China, purity >95%, conformed by HPLC). Commercially available reagents were used without further purification. ROS used in this study were prepared as follows. Superoxide ($O_2^{\bullet-}$) was generated from KO_2 in an anhydrous DMSO solution, and the concentration of $O_2^{\bullet-}$ was determined by the concentration of KO_2. H_2O_2 was diluted from a 30% aqueous solution. Hypochlorite (NaOCl) was diluted appropriately in 0.1 M NaOH aq. Singlet oxygen ($^1O_2$) was prepared using the ClO^-/H_2O_2 system (1:2). Tertbutyl hydroperoxide (TBHP) was diluted from a 70% aqueous solution, and peroxynitrite ($ONOO^-$) was prepared from a stock solution of 10 mM in 0.3 M NaOH. Fluorescence emission spectra and full-wavelength absorption spectra were performed on Tecan Spark 10 M Multimode Microplate Reader and Biotek Synergy H1. Confocal laser scanning microscope imaging was conducted with the Leica TCS SP2 confocal microscope. The two-photon (TP) images were acquired with the Olympus FV1200MPE with a 25× water objective. A Ti:sapphire laser was used to excite the specimen at 800 nm. ^1H NMR spectra were recorded at 400 MHz, respectively. HRMS was measured using a Thermo LCQ Deca XP Max mass spectrometer with ESI.

Fluorescence Responses of CGA to Various Concentrations of $O_2^{\bullet-}$ in Anhydrous DMSO.[38] Various concentrations of 10 mM KO_2 were added into various volumes of 1 mL DMSO to make the final concentrations of 0, 1.0, 2.0, 3.0, 4.0, and 5.0 μM. **CGA** was added to the solution to make the final concentration of 10 μM. Fluorescence intensity was measured by Tecan Spark 10 M Multimode Microplate Reader, λ_{ex} = 400 nm and λ_{em} = 440−800 nm.

The Selectivity of CGA.[39] The selectivity of **CGA** was studied. The production of $O_2^{\bullet-}$ free radicals was generated in the enzymatic xanthine oxidase (XO)/hypoxanthine (HPX) system at 37 °C. 50 μL of xanthine oxidase (XO, 5 U/890 μL) was added to 150 μL of 100 mM HEPES buffer (pH 7.4) to prepare the enzymatic solution. HPX was added into the enzymatic assay to make the final concentration of 1 mM, and **CGA** was added into the solution to make the final concentration of 10 μM. **CGA** was unperturbed upon the addition of various concentrations of reactive species and metal ions including K^+, Na^+, Ca^{2+}, Ni^{2+}, Zn^{2+}, Al^{3+}, Mg^{2+}, Mn^{2+}, and Li^+. $\lambda_{ex}/\lambda_{em}$ = 400 nm/480 nm.

Cell Culture. A375 (ATCC CRL-1619) as a human melanoma cell line was obtained from China Infrastructure of Cell Line Resources (Beijing, China). A375 cells were cultured in DMEM (Dulbecco's modified Eagle's medium) (Corning) containing 10% fetal bovine serum (Invitrogen) and 1% penicillin−streptomycin (Corning) at 37 °C under normoxia (95% air, 5% CO_2) or hypoxia (1% O_2, 94% N_2, and 5% CO_2).

Confocal imaging.[40] The A375 cells (0.3 mL, 1 × 10^5 cells/mL) were seeded into an eight-well chamber with sterile coverslips at the bottom. After reaching 80% confluence, the cells were incubated with 10 μM **CGA** for 30 min at 37 °C and the cell culture media were removed and washed with PBS two times. To induce upregulated $O_2^{\bullet-}$, 2-Me was used to treat the cells. The A375 cells were incubated with 10 μM **CGA** for 30 min at 37 °C after being pretreated with 0.1 μg/mL 2-Me for 15 min. Then, the cells were washed with PBS and the $O_2^{\bullet-}$scavenger Vc was given to the cells. All cells were observed with Leica TCS SP8 X Confocal Microscope using 63× oil immersion objective using a high-pressure He−Ne lamp and diode laser for excitation (λ_{ex} = 405 nm and λ_{em} = 430−530 nm).

Colocalization Experiments in A375 cells.[41] A375 cells were incubated with 10 μM **CGA** for 30 min and the corresponding commercial organelle markers (mitochondria: Mito Tracker Green (200 nM) and lysosome: Lyso Tracker Red DND-99 (500 nM)) for 30 min. Mito and Lyso Tracker were dissolved in DMSO with concentrations of 20 and 50 μM, respectively, to make a stock solution for use in fluorescence imaging experiments. After incubation, the cells were washed with PBS two times. Later, cells were observed with Leica TCS SP8 X Confocal Microscope using a 63 × oil immersion objective using a high-pressure He−Ne lamp and diode laser for excitation. **CGA** was excited at 405 nm, and the emissions were collected in the range of 430−530 nm; Mito Tracker Green was excited at 488 nm, and the fluorescence was monitored at 530−550 nm; and Lyso Tracker Red DND-99 was excited at 577 nm, and the fluorescence was monitored at 580−620 nm. The Pearson's coefficients were determined by ImageJ Software analysis.

Cell Viability Assay.[42] The cytotoxicity of **CGA** was measured by MTT assay *in vitro*. A375 cells (100 μL, 1 × 10^4 cells/mL) were transferred into 96-well plates, cultured for 12 h in a humidified 5% CO_2 atmosphere at 37 °C under normoxia or hypoxia, and then incubated with different concentrations (1.25−10 μM) of **CGA** for 72 h under normoxia or hypoxia. Subsequently, MTT (3-(4,5-dimethylthiazol-2-yl)-2,5-diphenyl tetrazolium bromide) solution (5 mg/mL, PBS) was then added to each well. After 4 h, the remaining MTT solution was removed and 150 μL of DMSO was added to each well. After 4 h incubation at 37 °C, the absorbance was measured at 490 nm with a Biotek Synergy H1. Cell viability was calculated according to the following formula: cell viability (%) = $(A - A_0)/(A_s - A_0) \times 100$, where A is the absorbance of the experimental group, A_s represents the absorbance of the control group, and A_0 stands for the absorbance of the blank group (no cells). The experiment was repeated three times.

For the colony formation assay, properly resuspended cells were randomly plated in a six-well plate at a density of 300 cells/well for 12 h under normoxia or hypoxia and then incubated with different concentrations (1.25−10 μM) of **CGA** under normoxia or hypoxia, respectively. After a 10-day incubation, cells were fixed by formalin and stained with 0.1% (W/V) crystal violet (SolarBio).

Measurement of Superoxide Anion Levels.[43] To detect cellular superoxide anion ($O_2^{\bullet-}$), fluorescent dye DHE (Beyotime Biotechnology) was used. In order to measure the $O_2^{\bullet-}$ production generated by treatments, A375 cells were incubated with **CGA** for 72 h under normoxia or hypoxia. The cells were harvested from each treatment and washed with PBS. After that, the cells were stained at 37 °C in the dark with 5 μM DHE. The stained cells were rinsed with wash buffer after 30 min and then resuspended in Tris−HCl buffer solution (0.1 M Tris−HCl, pH = 8.0). The fluorescence intensity of the cells stained with DHE was immediately measured by a flow cytometer (FACSVerse, BD). λ_{ex} = 535 nm and λ_{em} = 610 nm.

Western Blot Analysis. A375 cells were incubated with **CGA** for 72 h under normoxia or hypoxia. The cells were harvested from each condition and then washed with cold PBS. Cells were lysed with lysis buffer (SolarBio) on ice. After 30 min, cell lysates were centrifugated at 20,000 × *g* for 30 min at 4 °C. The supernatant was collected and quantified by using the Bradford protein assay (Yeasen). Samples were loaded into SDS-PAGE gel. Then, the proteins were transferred from the gel to the polyvinylidene fluoride membrane (Millipore). The membranes were then blocked with 5% skimmed milk powder at room temperature for 1 h. For primary antibodies incubation, the membranes were incubated overnight at 4 °C in a blocking buffer with diluted antibodies, including antibodies against p-AMPK (Cell Signaling Technology), AMPK (Cell Signaling Technology), and β-actin (Zhongshan Golden Bridge Biotechnology Co., Ltd.). The next day, washed with TBST buffer three times, the membranes were incubated with HRP-conjugated anti-goat (Zhongshan Golden Bridge Biotechnology Co., Ltd.) or anti-rabbit (Zhongshan Golden Bridge Biotechnology Co., Ltd.). Utilizing the Western blotting reagent,

https://doi.org/10.1021/acs.jmedchem.2c01317
J. Med. Chem. 2023, 66, 2498−2505

chemiluminescence was measured (Tanon Science & Technology Co., Ltd.).

Bioenergetics Measurements. Cells were plated in a XF24-well cell culture plates (Agilent, Santa Clara, CA, USA) at a density of 20,000 cells per well. The Real-Time ATP rate assay was performed independently in a Seahorse XF Analyzer (Agilent Technologies, Santa Clara, California), as recommended by the vendor. Briefly, A375 cells were incubated with **CGA** (0, 2.0 μM, 10 μM) for 6 h under normoxia and hypoxia. Then, these cells were incubated with unbuffered Seahorse XF Base medium supplemented with 10 mM glucose, 2 mM L-glutamine, and 1 mM sodium pyruvate and adjusted to pH 7.4. Cells were incubated for 1 h in a non-CO_2 incubator prior to sequential injections of mitochondrial stress or ATP test compounds. Results obtained were normalized for total cell number, using a standard cell counting assay, and normalized data was analyzed using an ATP Test generator from Agilent.

Determination of Extracellular Lactate. Extracellular acidification was measured by a Glycolysis Assay kit (Abcam). A375 cells treated with **CGA** (0, 5.0, 10, and 20 μM) were prepared in a 384-well plate for 72 h under normoxia or hypoxia. The extracellular acidification rate (ECAR) was measured through a fluorescent microplate reader at 620 nm (Biotek Synergy H1) as per the manufacturer's protocol.

Determination of Extracellular Oxygen Consumption. Extracellular oxygen consumption was measured using the Extracellular Oxygen Consumption Assay (Abcam). A375 cells treated with **CGA** (0, 5.0, 10, and 20 μM) were prepared in a 384-well plate for 72 h under normoxia or hypoxia. The OCR was measured through a fluorescent microplate reader at 650 nm (Biotek Synergy H1) as per the manufacturer's protocol.

Measurement of the Intracellular ATP Level. A357 cells were cultured into a 96-well plate at a density of 5×10^3 cells/well under various conditions. The ATP levels in cells were measured by a commercial ATP assay kit (Beyotime Biotechnology) according to the manufacturer's protocol. In brief, the assay buffer was mixed gently with the substrate at room temperature. Then, 100 μL mixed substrate buffer was added into wells and incubated at room temperature with shaking. After 15 min, luminescence intensity was measured using a microplate reader (Biotek Synergy H1).

Tumor Xenograft Model Studies.[44] Male athymic BALB/c-nu mice (8−10 weeks old, 20 g) were purchased from SPF Biotechnology Co., Ltd. (Beijing, China). All experiments were approved by the ethical committee and carried out following the guidelines of the Committee on Animals of the Institute of Materia Medica, Chinese Academy of Medical Sciences & Peking Union Medical College (Beijing, China, No. 00003649). 100 μL of 5−6 $\times$ 10^7/mL A375 melanoma cells was injected subcutaneously into the right flank of 6−8-week-old nude mice. Tumor-bearing mice were randomly grouped. When the tumor volume reached 100 mm^3, the treatments were started. These mice were injected intraperitoneally with Con (0.9% NaCl) or **CGA** (25 and 50 mg/kg) once daily. The length and width of tumors were measured every 3 days. At the end of the experiment, mice were first injected with Con or **CGA** intraperitoneally. After 1 h, mice were euthanized and tumors were harvested. Data including tumor and body weight were collected, and values were analyzed by GraphPad Prism 8.

Statistical Analysis. All results in this paper were performed in triplicate and presented graphically as mean ± standard deviation (SD). We calculated *P* values using one-way or two-way ANOVA. Differences were considered statistically significant at $^*P < 0.05$, $^{**}P < 0.01$, and $^{***}P < 0.001$. IC50 values were generated by nonlinear regression and analyzed using GraphPad Prism 8.

■ ASSOCIATED CONTENT

Supporting Information

The Supporting Information is available free of charge at https://pubs.acs.org/doi/10.1021/acs.jmedchem.2c01317.

Experimental procedures; compounds synthesis; ESR spectrum, computer simulations, geometry and spin density distribution studies of **CGA-SQ**$^\bullet$; additional fluorescence images; western blot, OCR, ECAR; NMR spectra; HPLC spectrum of **CGA**; references (PDF)

■ AUTHOR INFORMATION

Corresponding Authors

Xiaoguang Chen − *State Key Laboratory of Bioactive Substance and Function of Natural Medicines, Beijing Key Laboratory of Active Substance Discovery and Druggability Evaluation, Institute of Materia Medica, Chinese Academy of Medical Sciences and Peking Union Medical College, Beijing 100050, China*; Email: chxg@imm.ac.cn

Hai-Yu Hu − *State Key Laboratory of Bioactive Substance and Function of Natural Medicines, Beijing Key Laboratory of Active Substance Discovery and Druggability Evaluation, Institute of Materia Medica, Chinese Academy of Medical Sciences and Peking Union Medical College, Beijing 100050, China*; orcid.org/0000-0002-4760-6865; Email: haiyu.hu@imm.ac.cn

Authors

Qinghua Wang − *State Key Laboratory of Bioactive Substance and Function of Natural Medicines, Beijing Key Laboratory of Active Substance Discovery and Druggability Evaluation, Institute of Materia Medica, Chinese Academy of Medical Sciences and Peking Union Medical College, Beijing 100050, China*

Qingyang Zhang − *State Key Laboratory of Bioactive Substance and Function of Natural Medicines, Beijing Key Laboratory of Active Substance Discovery and Druggability Evaluation, Institute of Materia Medica, Chinese Academy of Medical Sciences and Peking Union Medical College, Beijing 100050, China*; orcid.org/0000-0003-4953-9536

Zhihui Zhang − *State Key Laboratory of Bioactive Substance and Function of Natural Medicines, Beijing Key Laboratory of Active Substance Discovery and Druggability Evaluation, Institute of Materia Medica, Chinese Academy of Medical Sciences and Peking Union Medical College, Beijing 100050, China*

Ming Ji − *State Key Laboratory of Bioactive Substance and Function of Natural Medicines, Beijing Key Laboratory of Active Substance Discovery and Druggability Evaluation, Institute of Materia Medica, Chinese Academy of Medical Sciences and Peking Union Medical College, Beijing 100050, China*

Tingting Du − *State Key Laboratory of Bioactive Substance and Function of Natural Medicines, Beijing Key Laboratory of Active Substance Discovery and Druggability Evaluation, Institute of Materia Medica, Chinese Academy of Medical Sciences and Peking Union Medical College, Beijing 100050, China*

Jing Jin − *State Key Laboratory of Bioactive Substance and Function of Natural Medicines, Beijing Key Laboratory of Active Substance Discovery and Druggability Evaluation, Institute of Materia Medica, Chinese Academy of Medical Sciences and Peking Union Medical College, Beijing 100050, China*

Jian-Dong Jiang − *State Key Laboratory of Bioactive Substance and Function of Natural Medicines, Beijing Key Laboratory of Active Substance Discovery and Druggability Evaluation, Institute of Materia Medica, Chinese Academy of Medical Sciences and Peking Union Medical College, Beijing 100050, China*

https://doi.org/10.1021/acs.jmedchem.2c01317
J. Med. Chem. 2023, 66, 2498−2505

Complete contact information is available at:
https://pubs.acs.org/10.1021/acs.jmedchem.2c01317

Notes

The authors declare no competing financial interest.

■ ACKNOWLEDGMENTS

We would like to sincerely acknowledge the assistance of the Imaging Core Facility, Technology Center for Protein Science, Tsinghua University, for the assistance using Olympus FV1000MPE, especially Ms. Yanli Zhang for her professional guidance in the animal imaging technology. We would also like to thank Prof. Shu Xu, Prof. Huaqing Cui, Dr. Ling-Ling Wu, and Xiang Wang in our institute for their experimental supports. The work of the Hu lab is funded by the National Natural Science Foundation of China (NSFC) projects (22122705, 22077139, 21907108) and CAMS Innovation Fund for Medical Sciences (CIFMS) (2022-I2M-2-002, 2022-I2M-1-014, 2021-I2M-1-054).

■ ABBREVIATIONS

ATCC, American Type Culture Collection; AMPK, activated protein kinase; ATP, adenosine triphosphate; CGA, chlorogenic acid; DMSO, dimethyl sulfoxide; DMEM, Dulbecco's modified Eagle's medium; ECAR, extracellular acidification rates; FBS, fetal bovine serum; HEPES, *N*-2-hydroxyethyl piperazine-*N*-2-ethane sulfonic acid; HPX, hypoxanthine; HRMS, high-resolution mass spectrometry; 2-ME, 2-methoxyestradiol; MTT, 3-(4,5-dimethylthiazol-2-yl)-2,5-diphenyltetrazolium bromide; NMR, nuclear magnetic resonance; OCR, oxygen consumption rates; PBS, phosphate-buffered saline; ROS, reactive oxygen species; TP, two-photon; TBHP, *tert*-butyl hydroperoxide; Vc, ascorbic acid; XO, xanthine oxidase; SOD, superoxide dismutase

■ REFERENCES

(1) Pan, C.; Li, B.; Simon, M. C. Moonlighting functions of metabolic enzymes and metabolites in cancer. *Mol. Cell* **2021**, *81*, 3760−3774.
(2) Schiliro, C.; Firestein, B. L. Mechanisms of metabolic reprogramming in cancer cells supporting enhanced growth and proliferation. *Cell* **2021**, *10*, 1056.
(3) Park, J. H.; Pyun, W. Y.; Park, H. W. Cancer metabolism: phenotype, signaling and therapeutic targets. *Cell* **2020**, *9*, 2308.
(4) Martínez-Reyes, I.; Chandel, N. S. Cancer metabolism: looking forward. *Nat. Rev. Cancer* **2021**, *21*, 669−680.
(5) Perillo, B.; Di Donato, M.; Pezone, A.; Di Zazzo, E.; Giovannelli, P.; Galasso, G.; Castoria, G.; Migliaccio, A. ROS in cancer therapy: the bright side of the moon. *Exp. Mol. Med.* **2020**, *52*, 192−203.
(6) Zhang, J.; Duan, D.; Song, Z. L.; Liu, T.; Hou, Y.; Fang, J. Small molecules regulating reactive oxygen species homeostasis for cancer therapy. *Med. Res. Rev.* **2021**, *41*, 342−394.
(7) Hayes, J. D.; Dinkova-Kostova, A. T.; Tew, K. D. Oxidative stress in cancer. *Cancer Cell* **2020**, *38*, 167−197.
(8) Cheung, E. C.; Vousden, K. H. The role of ROS in tumour development and progression. *Nat. Rev. Cancer* **2022**, *22*, 280−297.
(9) Sies, H.; Belousov, V. V.; Chandel, N. S.; Davies, M. J.; Jones, D. P.; Mann, G. E.; Murphy, M. P.; Yamamoto, M.; Winterbourn, C. Defining roles of specific reactive oxygen species (ROS) in cell biology and physiology. *Nat. Rev. Mol. Cell Biol.* **2022**, *23*, 499−515.
(10) Sena, L. A.; Chandel, N. S. Physiological roles of mitochondrial reactive oxygen species. *Mol. Cell* **2012**, *48*, 158−167.
(11) Sies, H.; Jones, D. P. Reactive oxygen species (ROS) as pleiotropic physiological signalling agents. *Nat. Rev. Mol. Cell. Biol.* **2020**, *21*, 363−383.
(12) Mailloux, R. J. An update on methods and approaches for interrogating mitochondrial reactive oxygen species production. *Redox Biol.* **2021**, *45*, No. 102044.
(13) Zhao, J.; Chen, J.; Ma, S.; Liu, Q.; Huang, L.; Chen, X.; Lou, K.; Wang, W. Recent developments in multimodality fluorescence imaging probes. *Acta Pharm. Sin. B* **2018**, *8*, 320−338.
(14) Hong, S.; Pawel, G. T.; Pei, R.; Lu, Y. Recent progress in developing fluorescent probes for imaging cell metabolites. *Biomed. Mater.* **2021**, *16*, No. 044108.
(15) Gao, P.; Pan, W.; Li, N.; Tang, B. Fluorescent probes for organelle-targeted bioactive species imaging. *Chem. Sci.* **2019**, *10*, 6035−6071.
(16) Bu, L.; Shen, B.; Cheng, Z. Fluorescent imaging of cancerous tissues for targeted surgery. *Adv. Drug Delivery Rev.* **2014**, *76*, 21−38.
(17) Xu, L.; Zhang, J.; Yin, L.; Long, X.; Zhang, W.; Zhang, Q. Recent progress in efficient organic two-photon dyes for fluorescence imaging and photodynamic therapy. *J. Mater. Chem. C* **2020**, *8*, 6342−6349.
(18) Helmchen, F.; Denk, W. Deep tissue two-photon microscopy. *Nat. Methods* **2005**, *2*, 932−940.
(19) Pawlicki, M.; Collins, H. A.; Denning, R. G.; Anderson, H. L. Two-photon absorption and the design of two-photon dyes. *Angew. Chem., Int. Ed.* **2009**, *48*, 3244−3266.
(20) Kim, H. M.; Cho, B. R. Small-molecule two-photon probes for bioimaging applications. *Chem. Rev.* **2015**, *115*, 5014−5055.
(21) Wu, L.; Liu, J.; Li, P.; Tang, B.; James, T. D. Two-photon small-molecule fluorescence-based agents for sensing, imaging, and therapy within biological systems. *Chem. Soc. Rev.* **2021**, *50*, 702−734.
(22) Singh, A. K.; Nair, A. V.; Singh, N. D. P. Small two-photon organic fluorogenic probes: sensing and bioimaging of cancer relevant biomarkers. *Anal. Chem.* **2022**, *94*, 177−192.
(23) Clifford, M. N.; Jaganath, I. B.; Ludwig, I. A.; Crozier, A. Chlorogenic acids and the acyl-quinic acids: discovery, biosynthesis, bioavailability and bioactivity. *Nat. Prod. Rep.* **2017**, *34*, 1391−1421.
(24) Clifford, M. N.; Kerimi, A.; Williamson, G. Bioavailability and metabolism of chlorogenic acids (acyl-quinic acids) in humans. *Compr. Rev. Food Sci. Food Saf.* **2020**, *19*, 1299−1352.
(25) Lu, H.; Tian, Z.; Cui, Y.; Liu, Z.; Ma, X. Chlorogenic acid: A comprehensive review of the dietary sources, processing effects, bioavailability, beneficial properties, mechanisms of action, and future directions. *Compr. Rev. Food Sci. Food Saf.* **2020**, *19*, 3130−3158.
(26) Xiao, H.; Zhang, W.; Li, P.; Zhang, W.; Wang, X.; Tang, B. Versatile fluorescent probes for imaging the superoxide anion in living cells and *in vivo*. *Am. Ethnol.* **2020**, *59*, 4216−4230.
(27) Zhang, W.; Zhang, J.; Li, P.; Liu, J.; Su, D.; Tang, B. Two-photon fluorescence imaging reveals a Golgi apparatus superoxide anion-mediated hepatic ischaemia-reperfusion signalling pathway. *Chem. Sci.* **2019**, *10*, 879−883.
(28) Cadenas, E. Mitochondrial free radical production and cell signaling. *Mol. Aspects Med.* **2004**, *25*, 17−26.
(29) Sohal, R. S.; Svensson, I.; Sohal, B. H.; Brunk, U. T. Superoxide anion radical production in different animal species. *Mech. Ageing Dev.* **1989**, *49*, 129−135.
(30) Heikkila, E.; Hermant, A.; Thevenet, J.; Bermont, F.; Kulkarni, S. S.; Ratajczak, J.; Santo-Domingo, J.; Dioum, E. H.; Canto, C.; Barron, D.; Wiederkehr, A.; De Marchi, U. The plant product quinic acid activates Ca^{2+}-dependent mitochondrial function and promotes insulin secretion from pancreatic beta cells. *Br. J. Pharmacol.* **2019**, *176*, 3250−3263.
(31) Zadra, G.; Batista, J. L.; Loda, M. Dissecting the dual role of AMPK in cancer: from experimental to human studies. *Mol. Cancer Res.* **2015**, *13*, 1059−1072.
(32) Trefts, E.; Shaw, R. J. AMPK: restoring metabolic homeostasis over space and time. *Mol. Cell* **2021**, *81*, 3677−3690.
(33) Zhao, Y.; Hu, X.; Liu, Y.; Dong, S.; Wen, Z.; He, W.; Zhang, S.; Huang, Q.; Shi, M. ROS signaling under metabolic stress: cross-talk between AMPK and AKT pathway. *Mol. Cancer* **2017**, *16*, 79.
(34) Huang, S.; Wang, L. L.; Xue, N. N.; Li, C.; Guo, H. H.; Ren, T. K.; Zhan, Y.; Li, W. B.; Zhang, J.; Chen, X. G.; Han, Y. X.; Zhang, J.

L.; Jiang, J. D. Chlorogenic acid effectively treats cancers through induction of cancer cell differentiation. *Theranostics* **2019**, *9*, 6745−6763.
(35) Mungai, P. T.; Waypa, G. B.; Jairaman, A.; Prakriya, M.; Dokic, D.; Ball, M. K.; Schumacker, P. T. Hypoxia triggers AMPK activation through reactive oxygen species-mediated activation of calcium release-activated calcium channels. *Mol. Cell. Biol.* **2011**, *31*, 3531−3545.
(36) Papandreou, I.; Lim, A. L.; Laderoute, K.; Denko, N. C. Hypoxia signals autophagy in tumor cells via AMPK activity, independent of HIF-1, BNIP3, and BNIP3L. *Cell Death Differ.* **2008**, *15*, 1572−1581.
(37) Guzy, R. D.; Hoyos, B.; Robin, E.; Chen, H.; Liu, L.; Mansfield, K. D.; Simon, M. C.; Hammerling, U.; Schumacker, P. T. Mitochondrial complex III is required for hypoxia-induced ROS production and cellular oxygen sensing. *Cell Metab.* **2005**, *1*, 401−408.
(38) Ding, Q.; Tian, Y.; Wang, X.; Li, P.; Su, D.; Wu, C.; Zhang, W.; Tang, B. Oxidative damage of tryptophan hydroxylase-2 mediated by peroxisomal superoxide anion radical in brains of mouse with depression. *J. Am. Chem. Soc.* **2020**, *142*, 20735−20743.
(39) Wang, Y.; Han, J.; Xu, Y.; Gao, Y.; Wen, H.; Cui, H. Taking advantage of the aromatisation of 7-diethylamino-4-methyl-3,4-dihydrocoumarin in the fluorescence sensing of superoxide anion. *Chem. Commun.* **2020**, *56*, 9827−9829.
(40) Zhang, Q.; Wang, Q.; Sun, Y.; Zuo, L.; Fetz, V.; Hu, H. Y. Superior fluorogen-activating protein probes based on 3-indole-malachite green. *Org. Lett.* **2017**, *19*, 4496−4499.
(41) Brennecke, B.; Wang, Q.; Haap, W.; Grether, U.; Hu, H.-Y.; Nazaré, M. DOTAM-based, targeted, activatable fluorescent probes for the highly sensitive and selective detection of cancer cells. *Bioconjugate Chem.* **2021**, *32*, 702−712.
(42) Dong, H.; Diao, H.; Zhao, Y.; Xu, H.; Pei, S.; Gao, J.; Wang, J.; Hussain, T.; Zhao, D.; Zhou, X.; Lin, D. Overexpression of matrix metalloproteinase-9 in breast cancer cell lines remarkably increases the cell malignancy largely via activation of transforming growth factor beta/SMAD signalling. *Cell Proliferation* **2019**, *52*, No. e12633.
(43) Dikalov, S. I.; Harrison, D. G. Methods for detection of mitochondrial and cellular reactive oxygen species. *Antioxid. Redox Signaling* **2014**, *20*, 372−382.
(44) Du, T.; Lin, S.; Ji, M.; Xue, N.; Liu, Y.; Zhang, Z.; Zhang, K.; Zhang, J.; Zhang, Y.; Wang, Q.; Sheng, L.; Li, Y.; Lu, D.; Chen, X.; Xu, H. A novel orally active microtubule destabilizing agent S-40 targets the colchicine-binding site and shows potent antitumor activity. *Cancer Lett.* **2020**, *495*, 22−32.

https://doi.org/10.1021/acs.jmedchem.2c01317
J. Med. Chem. 2023, 66, 2498−2505